Sequential Mechanism of Methane Dehydrogenation over Metal (Mo or W) Oxide and Carbide Catalysts†

Taijin Zhou,* Aimin Liu,‡ Yirong Mo,‡ and Hongbin Zhang

Department of Chemistry, and the State Key Lab of Physical Chemistry for the Solid Surface, Xiamen University, Xiamen 361005, P. R. China

Received: August 20, 1999; In Final Form: January 24, 2000

Methane activation in the absence of molecular oxygen over metallo-catalysts has been recognized as a potential catalytic process. In the present study, the density-functional theory (DFT) is employed to theoretically explore the mechanism of the nonoxidative dehydrogenation of methane on acid-promoted metal (Mo or W) oxides and carbide/zeolite catalysts. Various possible models of the catalyst are proposed. The structures of intermediate fragments together with CH_x species that adsorbed on the catalysts were optimized and analyzed. The results suggest that the transition metal species located on the bridged hydroxyl groups, Si(OH)Al of zeolites, is the activation center competent to cleave C−H bonds. Methane activation proceeds through the initial overlap of electron density of methane with vacant d-orbitals of the metallo-center of the catalyst, followed by the formation of a transition state in which a H−H bond distance is noticeably shortened. At last, a hydrogen molecule is eliminated and a bound carbene is then shaped. The H_2 evolution sequence can be described in a stepwise reaction: CH_4 + catalyst → H_4C−catalyst → H_2C−catalyst + H_2. The transition state of the adsorbed methane has a three-center−two-electron (2e−3c) bond, which is believed to be a key feature during the cleavage of two C−H bonds in the dehydrogenation process. The adsorbed CH_x species on the models of catalyst MoC_x[Si(O)Al] are comparable to pseudo-carbonium ions. Despite of the apparent differences in later stages, the initial steps in the dehydrogenation of methane on the MO_xC_y/HZSM-5 (M = Mo or W) catalysts share intrinsic properties with those of methane activation reactions in superacids.

Introduction

The dehydrogenation−aromatization of methane (DHAM) in the absence of O_2 has become one of the prospective processes for the utilization of natural gas resource. An attractive advantage of DHAM is that the yielded higher hydrocarbons can be easily separated from the reaction moiety. The byproduct, molecular hydrogen, is of great interest to industry since it is a clean energy source. Although the process is not thermodynamically favorable at low temperatures, it has become one of the frontiers in the field of methane activation chemistry. Compared to the oxidative coupling of methane (OCM), which is another developing process for the utilization of methane, DHAM is less complicated.

In the past few years, DHAM reactions over Mo/HZSM-5, MoO_3/ZSM-5, MoO_2/ZSM-5, MoO_2/HZSM-5, MoC_2/ZSM-5, MoC_2/HZSM-5, Mo−W/HZSM-5, Mo−Pt/HZSM-5, Mo−Ru/HZSM-5, and Mo−Co/HZSM-5 catalysts have been studied.[1−12] A highly active B-acid-promoted catalyst MO_xC_y/HZSM-5 (M = Mo or W) has been experimentally developed by one of us, on which both the rates of CH_4 conversion and benzene yield are about 1.4 times higher than those over the corresponding nonpromoted catalyst[3] (Table 1). Solymosi et al.[4] compared the interactions of methane with supported and unsupported molybdenum compounds (Mo, MoO_2, MoO_3, MoC_x). They have found that Mo_2C on ZSM-5 in high dispersion is a highly active and selective catalyst for the methane aromatization (the selectivity to benzene reaches 80−85% at a conversion of 6.0−7.0%). DHAM over a 2 wt % Mo^x/ZSM-5 catalyst has been reported.[5] Exposure of the catalyst to CH_4 or CH_4/H_2 at 700 °C reduces Mo ions to Mo_2C. The formation of Mo_2C is consistent with the time range of the initial activation period that generates ethylene and benzene, implying that a carbidic molybdenum species may be the active center for the methane activation and the consequent aromatization. XANES/EXAFS[6] and TG/DTA/Mass studies[8] have revealed that the zeolite-supported Mo oxide is endothermally converted to a Mo_2C cluster at around 682 °C in the presence of methane. The acidic site of Mo/HZSM-5 and the interaction between Mo species and HZSM-5 have been characterized by in situ FT-IR spectroscopy. Mo species are suggested mainly by sitting around the bridged hydroxyl groups

TABLE 1: Result of Activity Assays for Several Catalysts of Nonoxidative Dehydroaromatization of Methane[a]

catalyst sample	*T* (K)	conv *x*(CH_4)	selec, % C2	C3	Ben
HZSM-5	1018	0.1	88.2	0.0	11.8
Mo/Al_2O_3	1018	0.7	28.7	0.0	61.
Mo/SiO_2	1018	0.8	12.4	0.0	85.5
4%Mo/HZSM-5	1018	15.4	0.0	0.0	90.7
4%Mo-3.5%Zn−H_2SO_4/HZSM-5	1018	21.5	0.0	0.0	93.2
2%Mo-1.5%Zn−H_2SO_4/HZSM-5	1018	19.0	0.0	0.0	93.8
2%W-1.5%Zn−H_2SO_4/HZSM-5	1073	20.5	0.0	0.0	96.0
2.5%W-1.5%Zn−H_2SO_4/HZSM-5	1173	23.2	0.0	0.0	97.0

[a] Part of the data is taken from ref 3.

† Project supported by State Key Lab of Physical Chemistry for the Solid Surface, Xiamen University. A.M.L. acknowledges a research grant from the National Science Foundation of China (No. 29301004).

* To whom correspondence should be addressed at Xiamen University. Fax: +86-592-2183795. E-mail: tjzhou@xmu.edu.cn.

‡ On sabbatical leave. Current address: Department of Chemistry, University of Minnesota, Minneapolis, MN 55455.

10.1021/jp9929622 CCC: $19.00
Published on Web 04/19/2000

associated with silanol, Si(OH)Al.[2f] The structure and density of Mo and the acidic sites on the Mo-exchanged HZSM-5 catalysts have recently been characterized.[7] The maximum conversion rate of methane was so far achieved on the catalyst MoC_x/HZSM-5 with a Mo/Al ratio of 0.4. It is interpreted that both exchanged cations and residual Brønsted-acidic sites are required for the conversion of methane to the C_6^+ aromatics. All these results are in accord with a general knowledge that the acidic sites on Mo/HZSM catalysts, the channel structure of ZSM-5, the valence state of Mo species, and the Mo/Al/Si ratio are the factors responsible for the performance of the catalysts in the DHAM reaction. During the activation of methane, MoC_x sites are formed from MO_x/HZSM-5 and believed to be required for the catalytic C−H bond activation.

The activation of methane by superacids at mild temperatures is also a topic for experimental and theoretical studies. The similarities between this process and DHAM have attracted our attention. Hypercoordinated carbonium ions, such as CH_5^+, can be formed by protonating saturated hydrocarbons with superacids.[13] Choudhary and co-workers have developed a new approach for the methane activation over H-galloaluminosilicate (MFI) zeolite in the presence of alkene or higher alkane.[14] Methane can be highly activated and donate its own hydrogen to alkene, yielding higher hydrocarbons and aromatics (10−45%) with impressive conversion rates at a relatively low temperature range (400−600 °C). Knowledge on the parent cations in these systems is critical for the understanding of the low-temperature activation of carbocations. Protonated CH_5^+ might be regarded as the prototype of such a group of species. Various structures of CH_5^+ have been theoretically investigated at high levels.[15,16] In fact, CH_5^+ can be understood as a proton inserted into a C−H σ-bond of methane that leads to a unique three-center-two-electron (2e−3c) bond, in which two electrons are distributed around three nuclei. Previous studies have shown that most C_1 carbocations contain one or more 2e−3c bonds, and the H atoms involved in a 2e−3c bond can undergo bond rearrangement very readily.[17]

Despite the fact that there are many remarkable progresses from numerous independent studies, the mechanism of nonoxidative dehydrogenation of methane on Mo(W)/HZSM-5 is still far from clear. To monitor the design of DHAM catalysts of high activity and selectivity, we initiated a theoretical study on the mechanistic aspects of the DHAM reaction. A model for the B-acid-promoted carbide catalysts $(Mo[T]C[T]_3)^{\delta+}(Al[T]OSi[T])^{\delta-}$, is proposed and examined by means of the DFT method. Here Al, Si, C, and Mo all are T centers of tetrahedral structures. The Mo[T] inoculates three C[T]s with three covalent bonds. A 2e−3c bond over the complex of protonated methane and the catalyst is delineated in the present study. Analysis on the CH_x fragments over the DHAM catalysts is expected to provide an insight for the understanding of DHAM.

Calculation Details

Throughout the work, all calculations were carried with the Gaussian 98 program package.[18] Study on the zeolite structure and reactivity by using ab initio, DFT, and the combined quantum chemical−molecular mechanical (QM/MM) method is an effort that many other groups have embarked on.[19−25] Particularly, recent studies have shown that the physical and chemical properties of metal cations substituted into HZSM-5 can be reliably investigated by DFT calculations.[24] The Mo and W complexes[26] have been studied at the DFT (B3LYP, BLYP, B3PW91) level. The hybrid B3LYP method[27] has been convinced to provide excellent descriptions of various reaction profiles in terms of geometry, heats, and energy barrier heights.[28] Therefore, the hybrid DFT (such as B3LYP and BHandHLYP[27a]) method was used in the present work. For C, O, and H atoms, the 6-31G(d) basis set was employed, except for the calculations concerning the carbide model $MoMe_3$(AlOSi) and model complexes CH_xMoMe_3(AlOSi) where the Lanl2MB basis set was used for the methyl groups. For the transitional metals Mo and W, as well as Al and Si, the standard Lanl2DZ basis set and the corresponding effective core potentials (ECP)[29] were adopted. The outermost core orbitals of the transition metals that correspond to the ns^2np^6 configuration were treated explicitly along with the nd, $(n+1)$s, and $(n+1)$p valence orbitals. Various stationary points for the modeled species, which are characterized by vibrational frequency calculations, were optimized.

Results

Energetics of Various Dissociative Channels of CH_4 in the Absence of a Catalyst. To compare with the DHAM reaction, a series of reactions that may occur in the absence of a catalyst which otherwise resemble those of the nonoxidative dehydrogenation processes of methane have been calculated at the B3LYP/6-31G(d) level (eqs 1−8).

$$CH_4 \rightarrow CH_3^+ + H^- \qquad \Delta E = 361.6 \text{ kcal/mol}, \Delta H^{298} = 354.5 \text{ kcal/mol} \quad (1)$$

$$CH_4 \rightarrow CH_3 + H \qquad \Delta E = 112.8, \Delta H^{298} = 104.8 \quad (2)$$

$$CH_3^+ \rightarrow CH_2 + H^+ \qquad \Delta E = 207.4, \Delta H^{298} = 198.5 \quad (3)$$

$$CH_3 \rightarrow CH_2 + H \qquad \Delta E = 118.0, \Delta H^{298} = 111.6 \quad (4)$$

$$CH_4 \rightarrow CH_2 + H_2 \qquad \Delta E = 121.2, \Delta H^{298} = 112.1 \quad (5)$$

$$CH_4 \rightarrow (C_2H_4 + 2H_2)/2 \qquad \Delta E = 30.9, \Delta H^{298} = 25.9 \quad (6)$$

$$CH_4 \rightarrow (C_2H_6 + H_2)/2 \qquad \Delta E = 22.2, \Delta H^{298} = 18.5 \quad (7)$$

$$C_2H_4 \rightarrow C_6H_6/3 + H_2 \qquad \Delta E = -2.7, \Delta H^{298} = -6.7 \quad (8)$$

The heterolytic splittings of C−H bonds in reactions 1 and 3 are not energetically favored. Whereas the energy barriers for the homolytic splittings in the reactions 2 and 4 via hydrogen abstraction are apparently low. In principle, methane could be cleaved directly into CH_2 and H_2 at a single step (reaction 5). The reactions 6 and 7 demonstrate that dehydrodimerization of methane to ethene or ethane is modestly endothermic and should be favorable at high temperatures; while transformation from ethene to benzene (reaction 8) is thermodynamically favorable.

CH_4 and CH_5^+ under Superacidic Conditions. In strong acids, methane behaves as a nucleophilic base and is activated most probably via the formation of CH_5^+. The process (in parentheses are the point group symmetries) is strongly exothermic.

$$CH_4(T_d) + H^+ \rightarrow CH_5^+(C_s\text{-}1) \qquad \Delta E = -128.6, \Delta H^{298} = -125.3 \text{ kcal/mol} \quad (9)$$

In an ideal case, the approaching of proton (H^+) to CH_4 has no barrier, namely, the activation energy of the reaction 9 is zero. Figure 1 depicts four fully optimized structures of CH_5^+,

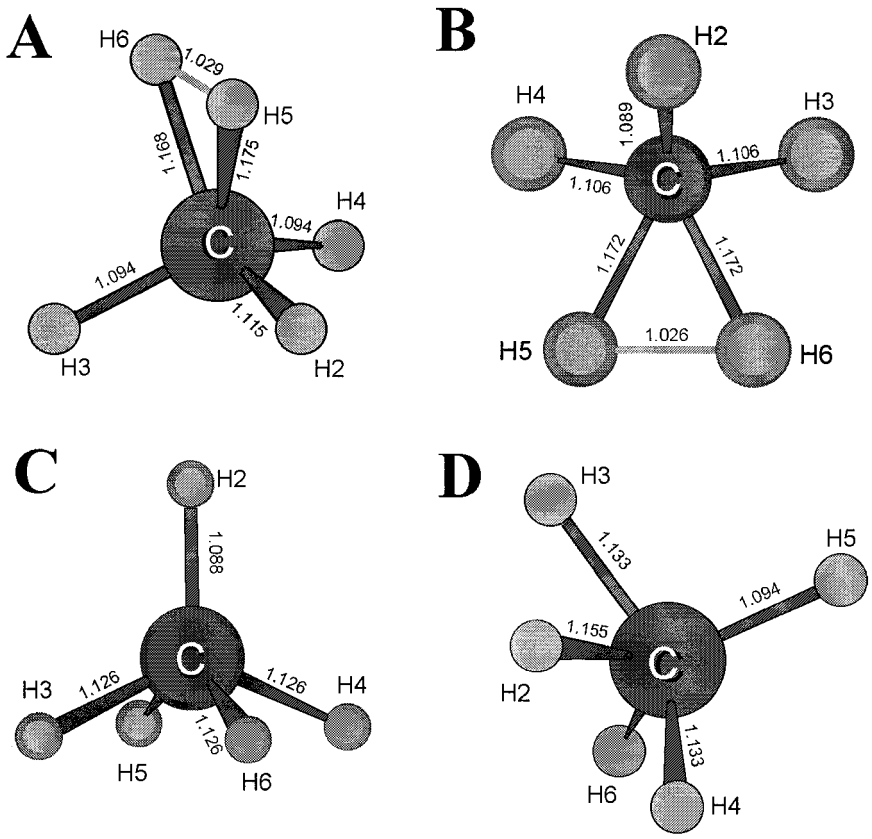

Figure 1. Conformers of CH_5^+. (A) $CH_5^+-C_s(1)$; (B) $CH_5^+-C_s(2)$; (C) $CH_5^+-C_{2v}(1)$; (D) $CH_5^+-C_{2v}(2)$. Bond lengths are indicated in Å.

TABLE 2: Absolute (in au) Energies (E) and Enthalpies (H^{298}) of CH_5^+ and CH_4 Structures

	B3LYP/6-31G(d)		CCSD(T)-R1215b	exptl[15b]
model	E	H^{298}	E	E
$CH_5^+-C_s(1)$	−40.723484	−40.668286	−40.723308	
$CH_5^+-C_s(2)$	−40.723484	−40.669137		
$CH_5^+-C_{2v}(1)$	−40.723276	−40.669256		
$CH_5^+-C_{2v}(2)$	−40.723252	−40.669728		
CH_4-T_d	−40.517663	−40.468620	−40.512666	−40.514
$CH_4-C_s(2)$	−40.314633	−40.275412		

with $C_s(1)$, $C_s(2)$, $C_{2v}(1)$, and $C_{2v}(2)$ symmetries, respectively. Computational results at the B3LYP/6-31G(d) level (see Table 2) show that the $C_s(1)$ structure corresponds to the minimum of CH_5^+, and the $C_s(2)$ structure has one imaginary frequency, which is a saddle point on the potential energy surface. The $C_{2v}(1)$ structure is also a minimum on the potential energy surface of CH_5^+. The $C_{2v}(2)$ structure is a saddle point. After the zero-point and thermal corrections, the enthalpy (H^{298}) of $C_s(2)$ is a little lower than that of the $C_s(1)$, and the enthalpy of $C_{2v}(2)$ is the lowest among all four conformations. The very trivial energy difference among these structures has been verified by the very accurate CCSD(T)-R12 method.[15b] CH_5^+ is thus known as a highly flexible molecule that is able to go through pseudo-rotating and hydrogen scrambling.[16,17] Although this rather complex dynamics makes its spectroscopy tough to discern, a complex of high-resolution infrared spectrum of CH_5^+ corresponding to the C−H stretching band in the 3−4 μm region has been reported. Furthermore, smaller barriers among the different structures of CH_5^+ may be raised from a recent infrared study.[30]

On the other hand, the presence of a H_2 moiety is a characteristic feature of the ground state of CH_5^+. The structural data of $CH_5^+-C_s(1)$ (Figure 1) show that the C−H5 and C−H6 bonds are activated, as evidenced from their longer bond lengths compared with the remaining C−H bonds. The interaction between H5 and H6 atoms is thus plausible. The C−H(5,6) unit therefore forms a 2e−3c bond. CH_5^+ is able to emancipate a H_2 molecule according to reaction 10.

$$CH_5^+ \rightarrow CH_3^+ + H_2 \qquad \Delta E = 42.4,\ \Delta H^{298} = 38.9 \text{ kcal/mol} \tag{10}$$

The CCSD(T)-R12 method with large basis sets (14s8p4d3f for C and 6s3p2d for H) results in the proton affinity of CH_4 (−133.2 kcal/mol) and the reaction energy including ZPVE between CH_3^+ and H_2 (−42 kcal/mol),[15b] both are in reasonable agreement with reactions 9 and 10.

In contrast to CH_5^+, the four C−H bonds in methane are highly stable. The three structures of T_d, C_{2v}, and $C_s(1)$ symmetries have almost the same energies. However, the $C_s(2)$ structure is a first-order saddle point in the potential energy surface.

$$CH_4(T_d) \rightarrow CH_4(C_s\text{-}2)$$
$$\Delta E = 127.4,\ \Delta H^{298} = 121.2 \text{ kcal/mol} \tag{11}$$

Because of the high activation energy of reaction 11, it is difficult to transform the structure of CH_4 from the ground state to those saddle points through pseudo-rotating and hydrogen scrambling.

DHAM Process over Metallo-Catalysts. In the present study, the nonoxidative dehydrogenation of methane on oxide/carbide catalyst MO_xC_y/HZSM-5 (M = Mo or W) is simulated, where the metal oxide/carbide prefers to deposit on the strong acidic sites of the HZSM-5 zeolite surface or channels.[3,7] It is clear that the origin of Brønsted acidity is the so-called bridging hydroxyl groups (AlOSi)H. These hydroxyl groups are initially formed when a silicon nucleus in a silica framework (tetrahedral structure, T site) is replaced by an aluminum and the resulting

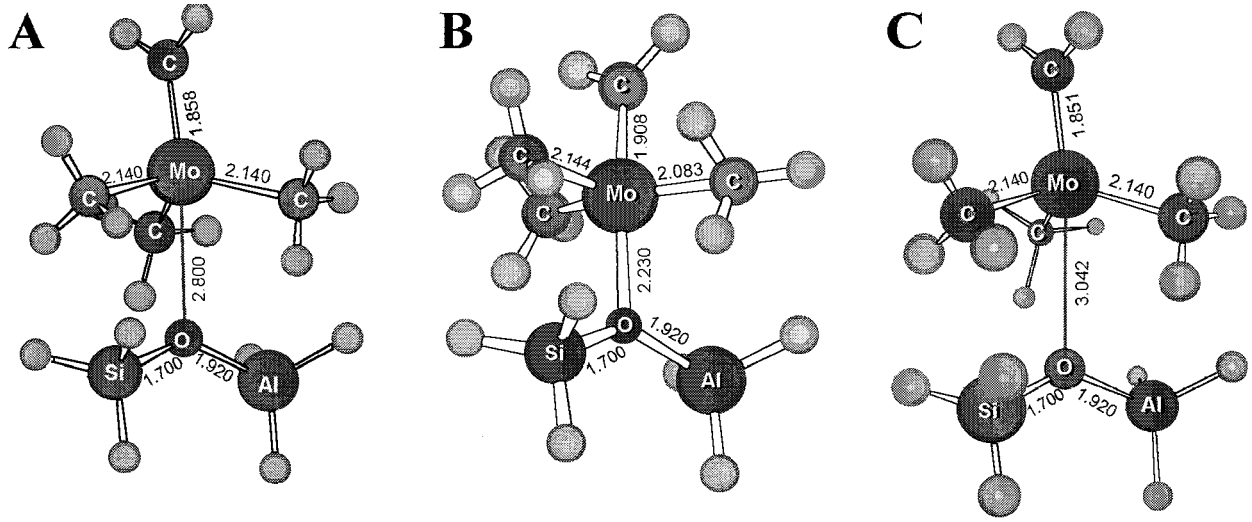

Figure 2. Adsorption of CH_2 on $MoMe_3$(AlOSi): (A) H_2CMoMe_3(AlOSi), **I**; (B) H_2CMoMe_3(AlOSi), **II**; (C) H_2CMoMe_3(AlOSi), **III**.

negative charge on the framework is compensated by adding a proton to any of the four oxygen atoms surrounding the aluminum atom.[21b] Iglesia and co-workers pointed out that the isolated MoO_x species might migrate into the zeolite channels via gas-phase or surface diffusion[7] and then could further react with H^+ at exchange sites and form a $Mo_2O_5^{2+}$ dimer and water molecule:

$$2MoO_3 + 2(AlOSi)H \rightarrow (AlOSi)Mo_2O_5(AlOSi) + H_2O \quad (12)$$

The $Mo_2O_5^{2+}$ species on $(AlOSi)Mo_2O_5(AlOSi)$ have ditetrahedral structures. This $Mo_2O_5^{2+}$ species can be reduced to form the active MoC_x complex during the initial stages of CH_4 conversion reactions.

$$(AlOSi)MO_x + CH_4 \rightarrow (AlOSi)MoC_x + H_2O \quad (13)$$

On the basis of the experimental facts shown above a carbide model of catalyst $(Mo[T]C[T]_3)^{\delta+}(Al[T]OSi[T])^{\delta-}$ was proposed. Subsequently, $(CH_x\ Mo[T]C[T]3)^{\delta+}(Al[T]OSi[T])^{\delta-}$, which represents the adsorption and activation of CH_x on the model, have been calculated and analyzed (Figures 2−4), where the Al, Si, C, and Mo in the catalyst models are T centers. The Mo[T] connects three C[T]s with three individual covalent bonds and has a lone pair as well as two residual dangling d-orbitals. The vacant characters of the dangling d-orbital of Mo are active centers and can adsorb CH_x. Obviously, the Al[T]OSi[T] unit has a negative charge ($\delta-$) and the $CH_xMo[T]C[T]_3$ unit has a positive charge ($\delta+$). The active sites are comparable with pseudo-carbocations. In fact, there have been many theoretical studies on the relationship between the acid strength and the structure of Al[T]OSi[T].[19−25] To simplify the calculations, some typical structural parameters were obtained from the literature: (a) the Si−O and Al−O bond lengths and Si−O−Al angle.[21b] The acidic and electrophilic characters of Al[T]OSi[T] depend on these geometric parameters. (b) The C−Mo bond length (2.14 Å) was taken from the EXAFS data.[8] The structural parameters deduced from the EXAFS fits are close to those of bulk β-Mo_2C, where the Mo ion has three neighboring carbon atoms at about 2.09 Å.[6,8] (c) Because the structure of MoC_x on HZSM-5 is close to the surface structure of Mo_2C and a cluster MoC_x locates above the oxygen atom of Si(O)Al,[2f,6−8,] we anticipate that the Mo−O distance is around the sum of Mo atom radii and O^{2-} ion radii (2.8 Å), which will be adopted in this work.

Since the elementary function of the Al[T]OSi[T] is very similar to that of a proton, we could replace the Al[T]OSi[T] fragment with H^+ and adopt models of $(HMoO_2)^+$ and $(HWO_2)^+$ to simulate the oxide catalysts of MoO_x/HZSM-5 and WO_x/HZSM-5, respectively. The positive ionic models, $(HMoO_2)^+$ and $(HWO_2)^+$, have dangling vacant metallo-d-orbital-active centers. Although these models are simplified, the intrinsic chemical properties of the metallo-center of the corresponding catalysts are mostly retained and, more importantly, these models are available for high-level computational analyses.

Adsorption of CH_x on the Model of Carbide $MoMe_3$-(AlOSi). A total of six models were used with the purpose of simulating adsorption and dehydrogenation of CH_4 as well as the formation of carbene on the carbide model of catalyst. They are (**a**) H_2CMoMe_3(AlOSi) (**I**, Figure 2A), (**b**) H_2CMoMe_3-(AlOSi) (**II**, Figure 2B), (**c**) H_2CMoMe_3(AlOSi) (**III**, Figure 2C), (**d**) H_4CMoMe_3(AlOSi) (Figure 3A), (**e**) H_4CMoMe_3-(AlOSi) (TS, Figure 3B), and (**f**) $MoMe_3$(AlOSi) (Figure 4), where Me represents a methyl group. In these models, the residual valence orbitals on Al(T), Si(T), and C(T) are saturated by hydrogen atoms. $(MoMe_3)^{\delta+}(AlOSi)^{\delta-}$ was analyzed by using several DFT schemes (B3LYP, BLYP, B3PW91, MPW1PW91, and BHandHLYP with the same basis set), and the results (Table 3) show that the DFT/ BHandHLYP scheme has the largest charge-transfer values δ, which are evaluated with the Mulliken and natural population analyses.[31] Since δ may be a key factor for the CH_x activation on the modeled catalysts, all of the six models (**a**−**f**) were calculated at the DFT/ BHandHLYP level with the geometry of C_s symmetry.

The charge-transfer value δ from H_xCMoMe_3 to AlOSi may act as a gauge of the acid strength of various models. Table 4 listed the δ values. Table 5 presents the natural bond orbitals (NBOs)[31] (with C23, O2), lone pairs, and vacant orbitals of Mo^+. The NBO analysis has been proved to be valuable for the understanding of chemical bonds during chemical reactions.[31] Formally, there is one electron transferred from Mo to Al to satisfy the T structure of Al. The formal charges of the Mo ion and the Al ion are +1 and −1, respectively. The numbers of valence electrons are 5 for Mo^+ and 4 for Al^-. Therefore, the Mo^+ ion has six valence orbitals and five valence electrons. Mo^+ in the above six model complexes is bonded with C11, C15, and C19. The bonds of Mo^+ with C23 and O2 vary with different models.

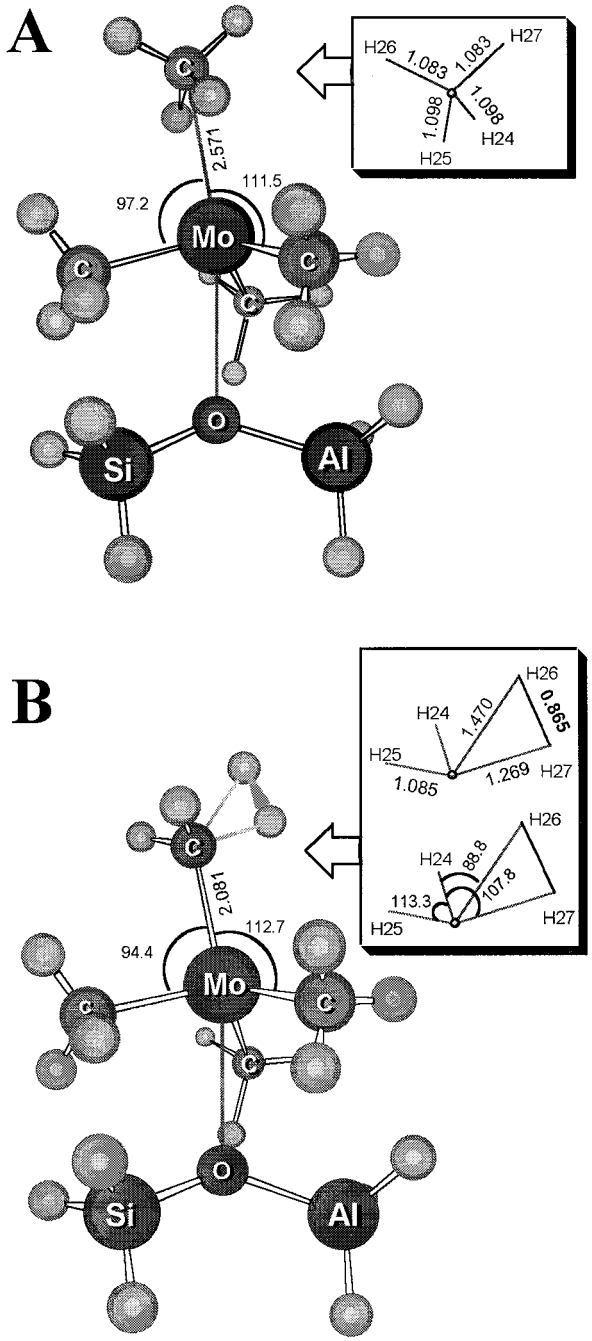

Figure 3. Adsorption of CH_2 on $MoMe_3$(AlOSi): (A) H_4-$CMoMe_3$(AlOSi); (B) H_2CMoMe_3(AlOSi), TS.

It is of interest to compare the geometry of model complex **a** (H_2CMoMe_3(AlOSi), **I**), **b** (H_2CMoMe_3(AlOSi), **II**), and **c** (H_2CMoMe_3(AlOSi), **III**) (Figure 2). The model complex **a** was only optimized at the H_2C unit, the model complex **b** was optimized at two units of H_2C and $MoMe_3$, and the model complex **c** was optimized at unit of H_2C as well as the Mo−O distance. The AlOSi unit was fixed for all model complexes.

It is clear that the relaxation distorts the $MoMe_3$ structures noticeably and in fact the Mo ion is pentagonally coordinated in model complex **b**, compared with a tetrahedron structure in model complex **a**. In model complex **b**, the Mo−O bond is formed in a way that the oxygen donates its lone electron pair to the vacant d-orbital of Mo (Table 5). Consequently, the distance of Mo and O in model complex **b** is significantly shortened to 2.17 Å from 2.80 Å of model complex **a**. In the meanwhile, the bond length C(23)−Mo is only slightly varied from 1.86 to 1.91 Å. In model complex **c**, however, the steric repulsion due to the fixed $MoMe_3$ fragment lengthens the Mo−O distance to 3.04 Å from 2.80 Å in model complex **a**.

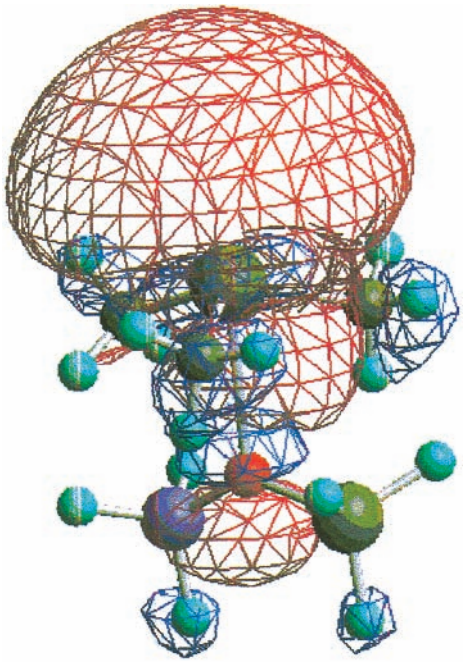

Figure 4. Lowest unoccupied molecular orbital (LUMO) of the model complex $MoMe_3$(AlOSi).

TABLE 3: Calculation Results of Different DFT Methods for Model $MoMe_3$(AlOSi)

		transferred charge value δ from $MoMe_3$ to AlOSi	
method	E (au)	Mulliken charge (e)	natural charge (e)
B3LYP	−270.2945589	0.601	0.730
B3PW91	−270.2792535	0.599	0.725
MPW1PW91	−270.2553284	0.620	0.749
BHandHLYP	−269.9509696	0.709	0.840
BLYP[a]	−270.0648163	0.453	0.570

[a] SCF calculation at BLYP level converged by setting the conversion = 4.

TABLE 4: Transferred Charge Value from the H_xCMoMe_3 Unit to the AlOSi Unit

model	Mulliken charge (e)	natural charge (e)
H_2CMoMe_3(AlOSi), **I**	0.754	0.894
H_4C $MoMe_3$(AlOSi)	0.726	0.846
H_4C $MoMe_3$(AlOSi), TS	0.750	0.878
$MoMe_3$(AlOSi)	0.709	0.840
H_2CMoMe_3(AlOSi), **II**	0.705	0.768
H_2CMoMe_3(AlOSi), **III**	0.797	0.916

However, recent experiments manifested that the carbidic molybdenum species on the zeolite surface is of a structure similar to that of the MoC_2 surface.[7,8] In other words, the noticeable distortion of the $MoMe_3$ species in model complex **b** may result from the cutoff of the surroundings. To mimic the real structures of catalysts, we recommend the structure of model complex **a**, where the $MoMe_3$ fragment is fixed to simulate the bonding pattern of Mo ion in real systems. The comparison between model complexes **a** and **b** also shows that the distortion of $MoMe_3$ has a very limited effect on the absorption of CH_2 species. Thus, model complex **a** is suitable for the theoretical study of DHAM.

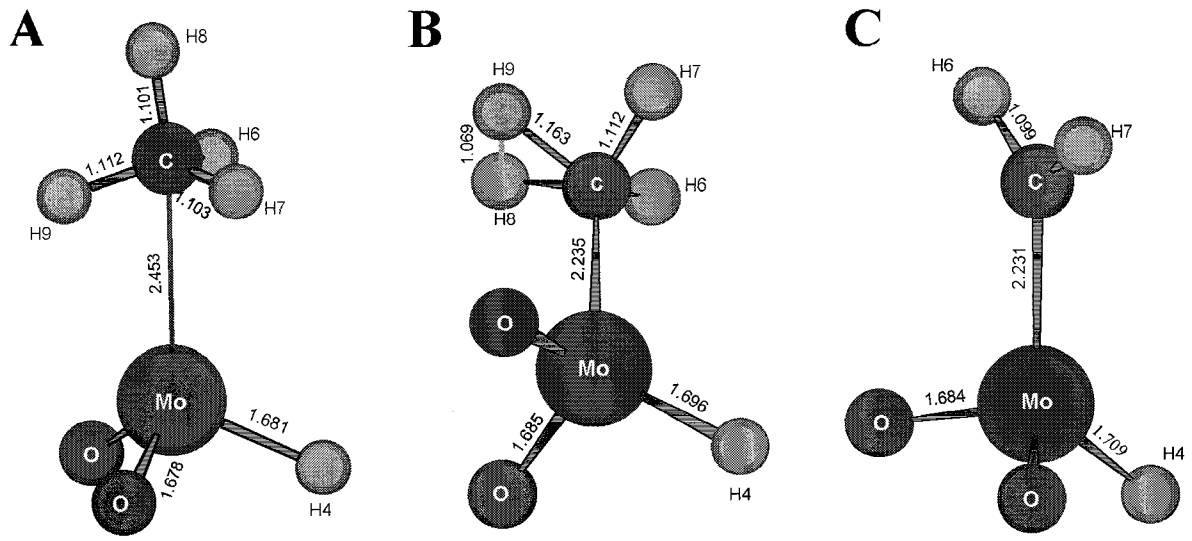

Figure 5. Adsorption of CH_x on MoO_2H^+: (A) $CH_4-C_s(1)$; (B) $CH_4-C_s(2)$; (C) CH_2.

TABLE 5: Natural Bond Orbital Analysis for Mo−C23 and Mo−O2 Bonds and the Lone Pair and Vacant Orbital of Mo

model	occ	atom %		hybrids %	atom %		hybrids %
$H_2CMoMe_3(AlOSi)$, **I**	1.973	Mo7	35.8	s(28.5)p(0.2)d(71.3)	C23	64.2	s(36.2)p(63.7)d(0.1)
	1.972	Mo7	56.2	s(0.5)p(0.6)d(98.9)	C23	43.8	s(1.3)p(98.6)d(0.1)
	0.252	Mo7	100	s(0.0)p(0.5)d(99.5)			
$H_4CMoMe_3(AlOSi)$	1.962	O2	91.8	s(14.3)p(85.7)	Mo7	8.2	s(25.6)p(1.4)d(73.1
	1.979	Mo	100	s(0.4)p(0.2)d(99.4)			
	0.225	Mo	100	s(0.0)p(0.1)d(99.9)			
$H_4CMoMe_3(AlOSi)$, TS	1.775	Mo	100	s(0.3)p(0.3)d(99.4)			
	0.437	Mo	100	s(52.6)p(0.9)d(46.6)			
	0.205	Mo	100	s(0.0)p(0.5)d(99.5)			
$MoMe_3(AlOSi)$	1.961	O2	92.0	s(11.6)p(88.4)	Mo	8.0	s(19.8)p(2.8)d(77.4)
	1.988	Mo7	100	s(1.4)p(0.3)d(98.3)			
	0.177	Mo7	100.	p(0.6)d(99.4)			
$H_2CMoMe_3(AlOSi)$, **II**	1.964	O2	94.7	s(0.00)p(100.)	Mo	5.3	s(0.0)p(0.4)d(99.6)
	1.951	Mo7	30.8	s(36.3)p(0.3)d(63.4)	C23	69.2	s(41.8)p(58.2)
	1.973	Mo7	63.5	s(0.0)p(0.1)d(99.9)	C23	36.5	s(0.1)p(99.8)d(0.1)
$H_2CMoMe_3(AlOSi)$, **III**	1.973	Mo7	36.7	s(27.0)p(0.1)d(72.9)	C23	63.3	s(35.2)p(64.8)d(0.1)
	1.972	Mo7	55.6	s(0.6)p(0.7)d(98.7)	C23	44.4	s(1.5)p(98.4)d(0.1)
	0.249	Mo7	100	s(0.0)p(0.5)d(99.5)			

The following reactions were considered from the calculation results on the model complex **a**, **d**, **e**, and **f**:

$$CH_4 + MoMe_3(AlOSi) \rightarrow H_4CMoMe_3(AlOSi)$$
$$\Delta E = 10.9,\ \Delta H^{298} = 12.4 \quad (14)$$

$$H_4CMoMe_3(AlOSi) \rightarrow H_4CMoMe_3(AlOSi)\ (TS)$$
$$\Delta E = 57.3,\ \Delta H^{298} = 53.1 \quad (15)$$

$$H_4CMoMe_3(AlOSi)\ (TS) \rightarrow H_2 + H_2CMoMe_3(AlOSi)$$
$$\Delta E = -50.6,\ \Delta H^{298} = -53.3 \quad (16)$$

The LUMO of model $MoMe_3(AlOSi)$ (Figure 4) is mainly a d-orbital of Mo. The methane activation proceeds through the initial overlap of the electron densities of two C−H bonds of methane with a vacant d-orbital on the transition metal center (reaction 14). The model complex **d** (Figure 3 A) is a minimum, although the energy of $H_4CMoMe_3(AlOSi)$ is higher than the sum of energy of CH_4 and $MoMe_3(AlOSi)$. Then the adsorbed methane rearranges to a transition state in which a H−H bond can form (reaction 15 and Figure 3B, TS). In the transition state, the distance between the two hydrogen atoms is 0.865 Å. Therefore, both of the H atoms are simultaneously activated, and a 2e−3c bond is formed. At last, the two H atoms are split from methane, eliminating hydrogen, and forming a bound carbene species (reaction 16 and Figure 2A). It is deduced from the calculation results that if relaxation distorts the $MoMe_3$ structures noticeably and the polarizing bond between Mo and O is formed, the charge-transfer value δ from H_xCMoMe_3 to AlOSi is only lightly decreased (see Table 4). Therefore, CH_4 still can be activated by residual d-orbital of Mo on the relaxed $MoMe_3$ and forming a Mo−C−H_2 multicenter bond with less and weak strength.

Activation of CH_4 on $(HMoO_2)^+$ and $(HWO_2)^+$. $(HMoO_2)^+$ and $(HWO_2)^+$ model complexes are fully optimized at the B3LYP level under the constraint of C_s symmetry. Obviously, it is not meaningful to compare the absolute eigenvalues of LUMO's in the positive ion models $(HMoO_2)^+$ and $MoMe_3$-(AlOSi); however, the principal components of LUMO's are the same, namely the d-orbitals of Mo. The electrons tend to shift from CH_4 to the vacant d-orbital of Mo when CH_4 is adsorbed on $(HMoO_2)^+$. Similar to CH_5^+, the $H_4C^{\delta+}(HMoO_2)^{+1-\delta}$ system has three possible structures of $C_s(1)$, $C_s(2)$, and C_1 symmetries. Since the C_1 and $C_s(1)$ structures of CH_4^{δ} $(HMoO_2)^{+1-\delta}$ have almost the same energies, only the $C_s(1)$ structure is focused here. The $C_s(2)$ structure lies above $C_s(1)$ by 42.3 kcal/mol. The geometries of CH_4 in $C_s(1)$ and $C_s(2)$ are very distinct; i.e., the H6−H7 is perpendicular to the H8−H9 in $C_s(1)$ whereas parallel in $C_s(2)$ (Figure 5). The bond distances between Mo and C are 2.45 Å ($C_s(1)$) and 2.24 Å

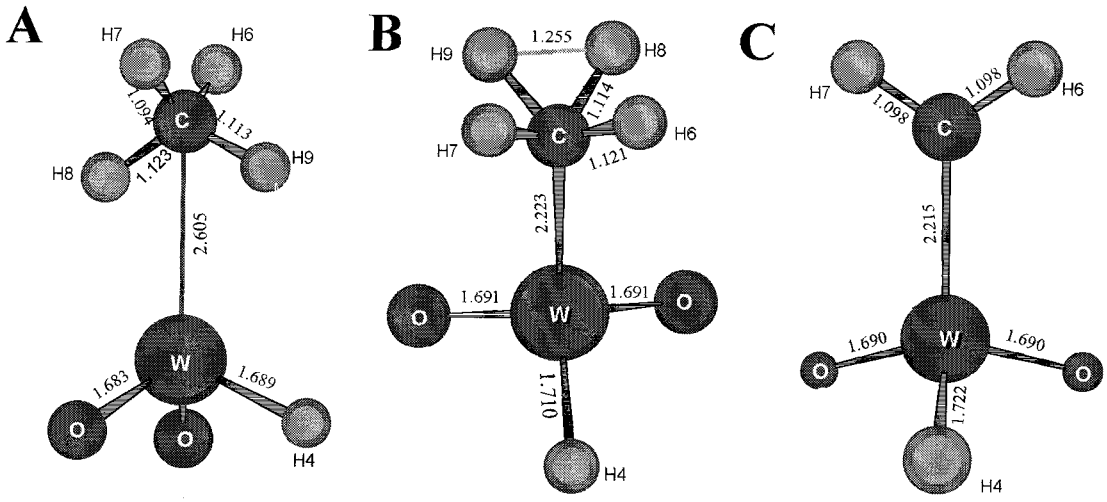

Figure 6. Adsorption of CH_x on WO_2H^+: (A) $CH_4-C_s(1)$; (B) $CH_4-C_s(2)$; (C) CH_2.

($C_s(2)$). These data show that Mo in the $C_s(1)$ is weakly bonded with C, H6, and H7, and there is no bonding interaction between H8 and H9. As of $C_s(2)$, Mo is bonded with C, but not bonded with H6 and H7 as in the $C_s(1)$ structure. The δ value of the $C_s(2)$ structure is bigger than that of the $C_s(1)$ structure, suggesting that the $C_s(2)$ structure tends to form a 2e−3c bond. The geometrical data also confirm the occurrence of a 2e−3c bond. For example, the H−H distance is 1.07 Å in the optimized $C_s(2)$ structure (Figure 5). In the $C_s(1)$ and C_1 structures, all four C−H bonds are 2c bonds. On the basis of the frequency calculations, $H_4C^{\delta}(HMoO_2)^{+1-\delta}-(C_s(1)$ or $C_1))$ is a minimum and $CH_4^{\delta}(HMoO_2)^{+1-\delta}-C_s(2)$ is a transition state. Compared with the monomers CH_4 and $(HMoO_2)^+$, the $C_s(1)$ structure is stabilized by −24.2 kcal/mol. In contrast, the $C_s(2)$ structure is destabilized by 18.1 kcal/mol. Similar to CH_5^+, the H_4C^{δ}-$(HMoO_2)^{+1-\delta}-C_s(2)$ system can easily liberate H_2. In the case of $H_2C^{\delta+}(HMoO_2)^{+1-\delta}$, the strength of the remaining two C−H bonds are enhanced due to the departure of two H atoms from C. The adsorption of CH_2 on $(HMoO_2)^+$ is stronger than that of CH_4 and the corresponding adsorption enthalpy of CH_2 is −62.6 kcal/mol.

The reactions of dehydrogenation of methane over $(HMoO_2)^+$ is formulated as

$$CH_4 + (HMoO_2)^+ \rightarrow (H_4C-MoO_2H)^+(C_s\text{-}1)$$
$$\Delta E = -23.9,\ \Delta H^{298} = -24.2 \quad (17)$$

$$(H_4C-MoO_2H)^+(C_s\text{-}1) \rightarrow (H_4C-MoO_2H)^+(C_s\text{-}2)$$
$$\Delta E = 46.0,\ \Delta H^{298} = 42.3 \quad (18)$$

$$(H_4C-MoO_2H)^+(C_s\text{-}2) \rightarrow H_2 + (H_2CMoO_2H)^+$$
$$\Delta E = 34.9,\ \Delta H^{298} = 31.4 \quad (19)$$

Because of the acidic and electrophilic characters of the model catalyst, when CH_4 approaches to the catalysts, the electrons of the C−H bond are partly transferred to the LUMO of $(HMoO_2)^+$, which is mainly the vacant d dangling orbitals of the Mo ion. As a result of the formation of such a Mo−C−H_2 multicenter bond, the $H_4C^{\delta}-cat^{1-\delta}-C_s(1)$ structure is generated. The C−H bonds become slightly activated in $H_4C^{\delta}-cat^{1-\delta}-C_s(1)$. The activation energy for the bond rearrangements from $C_s(1)$ to $C_s(2)$ is lower than that in the case of noncatalyzed CH_4. Because of the obstacle, the C−M bond is weaker in C_s-(1) than that in $C_s(2)$. The H8−H9 bond, which is perpendicular to the H6−H7 bond in $C_s(1)$, rotates 90° to the position of the H6−H7 bond. A $H_4C^{\delta}-cat^{1-\delta}-C_s(2)$ structure is hence formed. There is a 2e−3c bond in this $C_s(2)$ species, and all four H atoms are not bonded with the Mo ion. Although the TS is not the highest energy state in a halfway of up-going stairs, the C−H bonds involved in the 2e−3c can split at the same time so as the C−Mo and H−H bonds continuously strengthen and eventually generate the H_2C-cat and H_2 species.

Figure 6 shows the geometry of the $C_s(1)$ ground state and the $C_s(2)$ transition state of $H_4C^{\delta}(HWO_2)^{+1-\delta}$. The corresponding reactions are as follows:

$$CH_4 + (HWO_2)^+ \rightarrow (H_4C-WO_2H)^+(C_s\text{-}1)$$
$$\Delta E = -23.8,\ \Delta H^{298} = -24.2 \quad (20)$$

$$(H_4C-WO_2H)^+(C_s\text{-}1) \rightarrow (H_4C-WO_2H)^+(C_s\text{-}2)$$
$$\Delta E = 38.8,\ \Delta H^{298} = 34.2 \quad (21)$$

$$(H_4C-WO_2H)^+(C_s\text{-}2) \rightarrow H_2 + (H_2CWO_2H)^+$$
$$\Delta E = 36.0,\ \Delta H^{298} = 33.9 \quad (22)$$

The δ values (natural charges) are 0.166 for $H_4C^{\delta}(HWO_2)^{+1-\delta}-C_s(1)$, 0.359 for $H_4C^{\delta}(HWO_2)^{+1-\delta}-C_s(2)$, and 0.343 for $H_2C^{\delta}(HWO_2)^{+1-\delta}$. In the $C_s(2)$ structure, the C5−H8−H9 forms a 2e−3c bond where the distance of H8−H9 is 1.26 Å.

Discussion

Quantum chemical calculations play a key complementary role in obtaining molecular-level insight into catalytic mechanisms and, particularly for the structural or transitional features, have been much less accessible for spectroscopy, or their information content has not been developed. In the present work, we calculated the activation process of methane on the model catalysts H^+, $(HMO_2)^+$ (M = Mo or W), and $MoMe_3(AlOSi)$. In all three cases, the modeled catalysts have a vacant s or d manifold. The activation of methane has been concluded to proceed through overlap of electron densities of methane with vacant orbitals and the subsequent rearrangement of hydrogen atoms. Because of the electron transfer from CH_4 to the vacant orbitals of catalysts, a 2e−3c bond can be generated. On the other hand, the three model systems have different acid strength, therefore the 2e−3c bond character possesses apparent differences in different models. The sequence of the acid strength is $H^+ > (HMO_2)^+ > MoMe_3(AlOSi)$. The H^+ has the largest acid

strength, and therefore, the 2e−3c bond is a characteristic feature of the ground state of CH_5^+. In contrast, $H_4CMoMe_3(AlOSi)$ and $H_4C(HMO_2)^+$ have a 2e−3c bond only at the transitional state. The two hydrogen atoms comprising the 2e−3c bond of $H_4CMoMe_3(AlOSi)$ are active, and the dissociation of the C−H bond is easier to occur at the transition state of H_4CMoMe_3-(AlOSi). Due to the weak acid strength, the adsorbed CH_4 (or CH_2) on $MoMe_3(AlOSi)$ could be regarded as a pseudo-carbonium ion.

$(Mo[T]C[T]_3)^{\delta+}(Al[T]OSi[T])^{\delta-}$ is used in this study to simulate the MoC_x/HZSM-5 catalysts. MoO_3 with octahedral coordination is shown to be a precursor of the active catalytic species, and it is likely transformed to a tetrahedral structure at the acidic site of the zeolite surface or channels.[6−8] The oxides of Mo are reduced so as to form an active MoC_x species during the initial stages of methane conversion. We believe that the active Mo species should be a locally distorted T site coordinated by three carbons and an adsorbed CH_x.

On the basis of the calculation results from these model systems, the activation reaction sequence is proposed as follows:

$$CH_4 + MC_x/HZSM\text{-}5 \rightarrow H_2C^+-MC_x/HZSM\text{-}5 + H_2 \quad (23)$$

$$CH_4 + H_2C^+-MC_x/HZSM\text{-}5 \rightarrow H_2C^+-H_2C-MC_x/HZSM\text{-}5 + H_2 \quad (24)$$

The terminal C_2H_4 adsorbed on the catalyst can be liberated:

$$H_2C^+-H_2C-MC_x/HZSM\text{-}5 \rightarrow C_2H_4 + M^+C_x/HZSM\text{-}5 \quad (25)$$

The formation of H_2 is probably the first irreversible step (or steps) and the driving force up to this stage of the reaction. The transient product C_2H_4 is tuned and encouraged to further aromatize to benzene in the pore of the ZSM-5 zeolite under appropriate conditions:

$$3C_2H_4 \rightarrow C_6H_6 + 3H_2 \quad (26)$$

Alternatively, $H_2C^+-H_2C-MC_x$/HZSM-5 could react with methane via an oligomerization process:

$$CH_4 + H_2C^+-(H_2C)_n-MC_x/HZSM\text{-}5 \rightarrow H_2C^+-(H_2C)_{n+1}-MC_x/HZSM\text{-}5 + H_2 \quad (27)$$

The long-chain complex is capable of aromatization under assistance of the three-dimensional structure of the pore structure:

$$H_2C^+-(H_2C)_5-MC_x/HZSM\text{-}5 \rightarrow C_6H_6 + MC_x/HZSM\text{-}5 + 3H_2 \quad (28)$$

It is reasonable to suppose that the metal ion M^x (M = Mo or W) on HZSM-5 has d-orbital character above Fermi level, and methane is adsorbed through the electron transfer from the C−H bond to virtual d-orbitals of M^x. Therefore, the formation of a 2e−3c bond is the electronic factor for the multiple turnovers of dehydrogenation of methane, and the channel structure of ZSM-5 is the geometric factor to meet the critical requirements of aromatization.

One may question why the catalytic dehydrogenation of methane to $H_2 + CH_2$ in a single step is easier than to $H + CH_3$ or $H^- + CH_3^+$. Although the cleavage of two C−H bonds requires more energy than the splitting of a single C−H bond, formation of the H−H bond and H_2C−cat bond could compensate to the loss. Thus, the catalyst with high active metallo-d-orbital and electrophilic characters can activate CH_4, release H_2, and generate H_2C−cat at low activation energy. Moreover, the strong acidity of the catalysts would assist to strengthen the adsorption of CH_x and generate long-chain hydrocarbons but decrease the product selectivity to aromatics. Thus, a moderate acidity is more favorable for the DHAM catalyst. This thereby provides a rationale for the catalyst design.

The proposed scheme is consistent with the following experimental observations or common knowledge on DHAM: (1) The acidity of catalysts is conducive to the formation of the 2e−3c bond, and therefore, the DHAM activity of acid-promoted catalyst MO_xC_y/HZSM-5 (M = Mo or W) is significantly higher than that of nonpromoted catalyst MO_xC_y/ZSM-5[3] (see Table 1). (2) Methane is highly activated over strong acid catalyst H−GaAlMFI zeolitic at 400−600 °C, but the conversion of methane to higher hydrocarbons and aromatics demands the additional alkenes. However, the selectivity for aromatics is lower (10−45%) compared to the catalyst M^x/HZSM-5.[14] (3) In extremely strong acid solution at 80 °C, CH_5^+ and $C_nH_{2n+1}^+$ start lengthening at the expose of CH_4 in the absence of a catalyst. But benzene is not possible to form due to the fact that the number of H is $2n + 1$ in the lengthening reaction.[13] Thus, the acid-promoted catalyst MC_x/HZSM-5 and superacidic methane activation at relatively low temperature are correlated. (4) Although the activity of W catalyst is somewhat different from that of Mo, the mechanism of methane conversion on both systems would be the same.[3] (5) The metal ion is the active center, but its catalytic activity is affected by the Al[T]-OSi[T] structure and geometry in its coordinated sphere. Exposure of molybdenum oxide catalyst to a CH_4 or CH_4/H_2 mixture reduces Mo ion and produces Mo_2C species.[4−8] Therefore, the stability of the carbide catalyst is better than that of the oxide catalyst. This result sheds a light on the puzzle why those catalysts, containing molybdenum carbide phase and appropriate type and number of acid sites, are preferable for DHAM. The active phase at acid sites plays an important role in the steps of methane dehydrogenation and subsequent aromatization.

The fact that the present computational insights are in accord with those experimental data allows us to conclude the models of DHAM catalyst are reasonable choices for simulating the real MC_x/HZSM-5 (M = Mo, W) catalysts. The results therefore extend the knowledge of the DHAM process that no other model systems to date afford.

Supporting Information Available: Coordinates of the optimized CH_5^+ structures shown in Figure 1 are tabulated in Table 1S, A−D. Coordinates of the three different partly optimized $H_2CMoMe_3(AlOSi)$ structures shown in the Figure 2 are tabulated in Table 2S, A−C. The details of the optimized $H_4CMoMe_3(AlOSi)$ shown in Figure 3 are given in Table 3S, A,B. Model catalyst $MoMe_3(AlOSi)$ structure shown in Figure 4 is given in Table 4S. Coordinates of the optimized CH_x−MoO_2H^+ structures shown in Figure 5 are tabulated in Table 5S, A−C. Coordinates of the optimized CH_x−WO_2H^+ structures shown in Figure 6 are tabulated in Table 6S, A−C. This material is available free of charge via the Internet at http://pubs.acs.org.

References and Notes

(1) Bragin, O. V.; Vasina, T. V.; Preobrazhenski, A. V.; Minachev, K. M. *Tzv. Akad. Nauk SSSR Ser Khim.* **1982**, 954; also **1989**, 750.

(2) (a) Wang, L.; Tao, L.; Xie, M.; Xu, G.; Huang, J.; Xu, Y. *Catal. Lett.* **1993**, *21*, 35. (b) Xu, Y.; Liu, S.; Wang, L.; Xie, M.; Guo, X. *Catal.*

Lett. **1995**, *30*, 135. (c) Wong, S. T.; Xu, Y.; Wang, L.; Xie, M. *Catal. Lett*. **1996**, *38*, 39. (d) Chen, L.; Lin, L.; Xu, Z.; Li, X.; Zhang, T. *J. Catal.* **1995**, *157*, 190. (e) Shu, Y.; Xu, Y.; Wong, S. T.; Wang, L.; Guo, X. *J. Catal*. **1997**, *170*, 11. (f) Liu, W.; Xu, Y. *J. Catal.* **1999**, *185*, 386. (g) Jiang, H.; Wang, L. S.; Cui, W. Xu, Y. D. *Catal. Lett.* **1999**, *57*, 95. (h) Xu, Y.; Liu, W.; Wong, S. T.; Guo, X. X. *Catal. Lett.* **1996**, *40*, 207.

(3) (a) Zeng, J. L.; Xiong, Z. T.; Zhang, H. B.; Lin, G. D.; Tsai, K. R. *Catal. Lett.* **1998**, *53*, 119. (b) Zeng, J. L.; Xiong, Z. T.; Lin, G. D.; Yu L.; Zhang, H. B. *Acta Phys. Chem. Sin.* **1998**, *14*, 394.

(4) (a) Solymosi, F.; Erdohelyi, A.; Szoke, A. *Catal. Lett.* **1995**, *32*, 43. (b) Solymosi, F.; Szoke, A. *Catal. Lett*. **1996**, *39*, 157. (c) Solymosi, F.; Cserenyi, J.; Szoke, A.; Bansagi, T.; Oszko, A. *J. Catal*. **1997**, *165*, 150. (d) Solymosi, F.; Szoke, A. *Appl. Catal. A* **1999**, *166*, 225.

(5) Dingjun, W.; Jack, H. L. A.; Michael, P. R. *J. Catal.* **1977**, *169*, 347.

(6) Zhang, J. Z.; Long, M. A.; Howe, R. F. *Catal. Today* **1998**, *44*, 293.

(7) Borry, R. W.; Kim, Y. H.; Huffsmith, A.; Reimer, J. A.; Iglesia, E. *J. Phys. Chem. B* **1999**, *103*, 5787.

(8) Liu, S. T.; Wang, L.; Ohuishi, R.; Ichikawa, M. *J. Catal*. **1999**, *181*, 175.

(9) Ohnishi, R.; Liu, S. T.; Dong, O.; Wang, L.; Ichikawa, M. *J. Catal.* **1999**, *182*, 92.

(10) Pierella, L. B.; Wang, L. S.; Anunziata, O. A. *React. Kinet. Catal. Lett.* **1997**, *60*, 101.

(11) Zhang, C. L.; Li, S. A.; Yuan, Y.; Zhang, W. X.; Wu, T. H.; Lin, L. *W. Catal. Lett*. **1998**, *56*, 207.

(12) Chen, L. Y.; Lin, L. W.; Xu, Z. S. *Catal. Lett*. **1996**, *39*, 169.

(13) (a) Olah, G. A.; Schlossberg, R. H. *J. Am. Chem. Soc.* **1968**, *90*, 2726. (b) Olah, G. A.; Klopman, G.; Schlossberg, R. H. *J. Am. Chem. Soc.* **1969**, *91*, 3261.

(14) Choudhary, V. R.; Kinage, A. K.; Choudhary, T. V. *Science* **1997**, *275*, 1286.

(15) (a) Schreiner, P. R.; Kim, S. J.; Schaefer, H. F.; Schleyer, P. V. R. *J. Chem. Phys*. **1993**, *99*, 3716. (b) Muller, H.; Kutzelnigg, W.; Noga, J.; Klopper, W. *J. Chem. Phys*. **1997**, *106*, 1863.

(16) (a) Scuseria, G. E. *Nature* **1993**, *366*, 512. (b) Marx, D.; Parrinello, M. *Nature* **1995**, *375*, 216.

(17) Rasul, G.; Prakash, G. K. S.; Olah, G. A. *Proc. Natl. Acad. Sci. U.S.A.* **1997**, *94*, 11159.

(18) Frisch; M. J.; Trucks, G. W.; Schlegel, H. B.; Gill, P. M. W.; Johnson, B. G.; Robb, M. A.; Cheeseman, J. R.; Keith, T.; Petersson, G. A.; Montgomery, J. A.; Raghavachari, K.; Al-Laham, M. A.; Zakrzewski, V. G.; Ortiz, J. V.; Foresman, J. B.; Peng, C. Y.; Ayala, P. Y.; Chen, W.; Wong, M. W.; Andres, J. L.; Replogle, E. S.; Gomperts, R.; Martin, R. L.; Fox, D. J.; Binkley, J. S.; Defrees, D. J.; Baker, J.; Stewart, J. P.; Head-Gordon, M.; Gonzalez, C.; Pople, J. A. *Gaussian 98*, Revision A.3; Gaussian, Inc.: Pittsburgh, PA, 1998.

(19) Kazansky, V. B.; Frash, M. V.; Vansanten, R. A. *Catal. Lett*. **1994**, *28*, 211.

(20) Redondo, A.; Hay, P. *J. Phys. Chem.* **1993**, *97*, 11754.

(21) (a) Hill, J. R.; Sauer, J. *J. Phys. Chem. A* **1994**, *98*, 1238. (b) Hill, J. R.; Sauer, J. *J. Phys. Chem.* **1995**, *99*, 9536.

(22) Fujino, T.; Kashitani, M.; Kondo, J. N.; Domen, K.; Hirose, C.; Ishida, M.; Goto, F.; Wakbayashi, F. *J. Phys. Chem.* **1996**, *100*, 11649.

(23) Sinclair, P E.; Vries, A.; Sherwood, P. Richard, C.; Catlow, A. *J. Chem. Soc., Farday Trans*. **1998**, *94*, 3401.

(24) Rice, M. J.; Chakraborty, A. K.; Bell, A. T. *J. Phys. Chem. A* **1998**, *102*, 7498.

(25) Vries, A. H.; Sherwood, P.; Collins, S. J.; Rigby, A. M.; Rigutto, M.; Kramer, G. J. Redondo, A.; Hay, P. *J. Phys. Chem. B* **1999**, *103*, 6133.

(26) Orlova, G.; Scheiner, S. *J. Phys. Chem. A* **1998**, *102*, 260.

(27) (a) Becke, A. D. *J. Chem. Phys.* **1993**, *98*, 5648. (b) Lee, C.; Yang, W.; Parr, R. G. *Phys. Rev.* **1988**, b37, 785.

(28) (a) Baker, J.; Muir, M.; Andzelm, J.; Scheiner, A. In *Chemical Applications of Density-Functional Theory*; Laird, B. B., Ross, R. B., Ziegler, T., Eds.; ACS Symposium Series 629; American Chemical Society: Washington, DC, 1996. (b) Yoshizawa, K.; Shiota, Y.; Yamabe, T. *J. Am. Chem. Soc*. **1999**, *121*, 147.

(29) Hay, P. J.; Wadt, W. R. *J. Chem. Phys.* **1985**, *82*, 299.

(30) Edmund, T. W.; Jian, T.; Takeshi, O. *Science* **1999**, *284*, 135.

(31) (a) Weinhold, F.; Carpenter, J. E. *The Structure of Small Molecules and Ions*; Plenum Press: New York, 1988; p 227. (b) Carpenter, J. E.; Weinhold, F. *THEOCHEM* **1988**, *169*, 41.